J. Fluid Mech. (2025), *vol.* 1018, A15, doi:10.1017/jfm.2025.10386

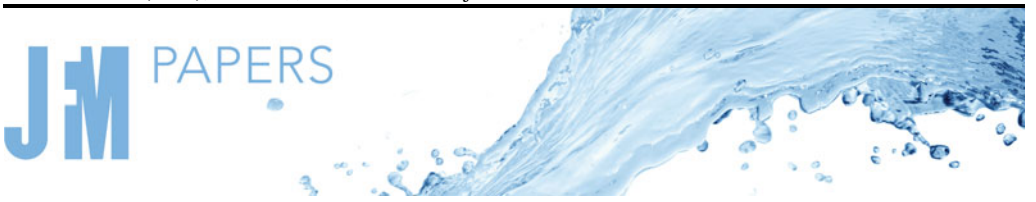

Oscillating flow in liquid metal vertical convection under the influence of a horizontal magnetic field

Sylvie Su[1,2], **Sanjay Singh**[1], **Sven Eckert**[1] **and Tobias Vogt**[1]

[1]Helmholtz-Zentrum Dresden-Rossendorf, Dresden 01328, Germany

[2]CORIA-UMR 6614 - Normandie Université, CNRS, INSA de Rouen, Saint Etienne du Rouvray 76800, France

Corresponding author: Sylvie Su, sylvie.su@coria.fr

(Received 12 August 2024; revised 29 April 2025; accepted 25 May 2025)

The effect of a horizontal magnetic field on heat transport and flow structures in vertical liquid metal convection (Prandtl number $Pr \approx 0.03$) is investigated experimentally. The experiments are carried out for Rayleigh numbers in the range of $1.48 \times 10^6 \leqslant Ra \leqslant 3.54 \times 10^7$ and Chandrasekhar numbers in the range of $2 \times 10^2 \leqslant Q \leqslant 1.86 \times 10^6$, as well as for the non-magnetic case ($Q = 0$). Measurements of the heat transport show a rise in the Nusselt number at low and moderate magnetic field strengths up to an optimum value of Q, before a further increase in the magnetic field leads to a decrease in the transport properties. By applying simultaneous velocity and temperature measurements, we are able to identify three different oscillatory flow regimes for $10^{-5} < Q/Ra < 0.5$ and assign them to the respective heat transfer characteristics. In the range $10^{-5} > Q/Ra > 10^{-3}$, first evidence of a transition to anisotropic flow structures caused by the magnetic field is visible. Two strongly oscillatory regimes are identified, where the energy is either distributed around a dominant frequency ($10^{-3} > Q/Ra > 10^{-2}$), or strongly concentrated on a single frequency ($10^{-2} > Q/Ra > 0.5$). The dominating frequency increases with the Rayleigh number according to $Ra^{0.71\pm0.02}$. This flow structure based regime separation correspond to changes of both the heat transfer through the Nusselt number and mass transfer through the Reynolds number.

Key words: magneto convection

1. Introduction

Thermally driven flows are widespread and relevant in nature, especially in geophysical and astrophysical systems, as well as in everyday life and industrial applications. The canonical configuration to study this type of flows is the Rayleigh–Bénard convection (RBC), where an encased fluid is heated from below, and cooled from the top (Bodenschatz, Pesch & Ahlers 2000; Ahlers, Grossmann & Lohse 2009). The thermal driving force is characterised by the Rayleigh number $Ra_H \equiv \alpha g \Delta T H^3/(\kappa \nu)$, where α, is the isobaric thermal expansion coefficient of the fluid, ν its the kinematic viscosity, κ its the thermal diffusivity, ΔT is the imposed temperature difference between the top and bottom plates, H is the gap between them and g is the gravitational acceleration. As a closely related configuration, vertical convection (VC) represents many technical processes, where two opposite vertical walls are heated and cooled (e.g. Batchelor 1954). In contrast to RBC, VC is always unstable, i.e. even the smallest temperature gradients cause the onset of flow. Numerical simulations and experimental data (Zwirner *et al.* 2022) have shown that the vertical length of the heated/cooled plate L is more suitable as characteristic length scale than the horizontal distance H because this leads to a better collapse of the Nu and Re data as functions of Ra, for moderate aspect ratios L/H. This Rayleigh number definition $Ra \equiv \alpha g \Delta T L^3/(\kappa \nu)$ is also used in this present study. A systematic theory for the scaling of the Nusselt number Nu and of the Reynolds number Re has been developed for RBC by Grossmann & Lohse (2000, 2002) and extended for VC by Ng *et al.* (2015), Shishkina (2016) and Ching (2023). The container aspect ratio $\Gamma \equiv L/H$ influences the flow organisation. It has been shown for both RBC and VC that different flow structures emerge in $\Gamma \leqslant 1$ and $\Gamma \gg 1$ (Pandey, Scheel & Schumacher 2018; Stevens *et al.* 2018).

Another parameter of interest for convective systems is the Prandtl number $Pr \equiv \nu/\kappa$. The majority of studies on thermally driven convection have focused on high Prandtl number fluids $Pr \gtrsim 1$, mostly air and water (e.g. Chen & Pearlstein 1989; Wang, Lohse & Shishkina 2021). However, structures and the dynamics of the convective flow are vastly different in low-Pr fluids ($Pr \ll 1$) (Vogt *et al.* 2018; Zürner *et al.* 2018; Zwirner *et al.* 2022; Teimurazov *et al.* 2023). An important property of low-Pr fluids is their high electrical conductivity, which results in an intensive interaction with external magnetic fields. The application of a direct current (DC) magnetic field is supposed to form new flow regimes and to modify the momentum and heat transport.

On the laboratory scale, the Chandrasekhar number $Q \equiv Ha^2 \equiv B^2 L^2 \sigma/\mu$ is the governing parameter to quantify the influence of a steady magnetic field on the fluid flow. It gives the ratio of electromagnetic to viscous forces, where B is the magnetic field intensity, σ is the electrical conductivity and $\mu = \rho\nu$ is the dynamic viscosity with ρ as the density of the fluid. The non-magnetic case of liquid metal VC in a parallepipedic cavity has been studied by analytical methods (Henry & BenHadid 2007; Medelfef *et al.* 2019) and numerical simulations (Henry & Buffat 1998).

Different configurations can be distinguished in the case of magnetic VC: the magnetic field can be aligned either parallel or perpendicular to the temperature gradient (parallel to the heating/cooling plates). A number of studies are devoted to the latter situation of a so-called transverse magnetic field with two further options, where the magnetic field can be aligned parallel or perpendicular to the direction of the gravity vector. An analytical solution for the configuration of a vertical magnetic field was provided by Garandet, Alboussiere & Moreau (1992) and confirmed by both experimental data (Okada & Ozoe 1992) and numerical simulations (Alchaar, Vasseur & Bilgen 1995). For the case of a horizontal magnetic field parallel to the heating/cooling walls, it has been shown that this is least effective in suppressing the main circulation (Ozoe & Okada 1989).

Such a situation is relevant for fusion reactors and has been studied numerically for various geometries (Wang *et al.* 2010; Kakarantzas *et al.* 2017; Wang & Zhou 2019; Masuda *et al.* 2023). Related experimental studies for low Pr fluids have been reported using liquid Gallium (Okada & Ozoe 1992; Tagawa & Ozoe 1998), mercury (Authié *et al.* 2003) and GaInSn (Wang, Meng & Ni 2017). Most of the studies focus on the magnetic field effects on the global heat transport by measuring the Nusselt number Nu. Enhanced heat transfer has been reported at moderate Hartmann numbers (Ha) by Tagawa & Ozoe (1997, 1998) and Authié *et al.* (2003). Similar behaviour is also known for RBC (Vogt *et al.* 2021). There are, to our knowledge, few studies with a transverse magnetic field in RBC, as the preferred configuration is with the magnetic field applied vertically, i.e. parallel to the thermal gradient (e.g. Garandet *et al.* 1992; Yan *et al.* 2019; Bader & Zhu 2023).

It is assumed that the presence of a magnetic field increases the coherent properties of the flow due to a suppression of small-scale turbulence. The flow is restructured and reaches an optimal state in which the Joule dissipation is minimised (Davidson 1995). Experimental investigations of the local properties of VC have only been carried out in rare cases to date. A first step in this direction was attempted by Derebail & Koster (1997), who visualised the temperature field and derived information on the global flow structure from the temperature data. A few studies report on flow measurements in liquid metal convection without and with a magnetic field (Zürner *et al.* 2018; Authié *et al.* 2003; Wang *et al.* 2017), but are mostly limited to collecting time-averaged data on the main circulation.

In the present work, liquid metal experiments are performed to investigate flow structures in VC under the influence of a horizontal magnetic field perpendicular to the temperature gradient. We aim to characterise both the main circulation, any secondary flow and their temporal dynamics.

2. Experimental set-up

A schematic drawing of the experimental set-up is shown in figure 1. The experiments are carried out using the eutectic alloy GaInSn, which is liquid at room temperature and has a Prandtl number of $Pr \approx 0.03$ (see Plevachuk *et al.* 2014 for data on its thermophysical properties). The liquid metal is contained in a rectangular vessel with a volume of $L_y \times L_z \times H = L^2 \times H = 200\,\text{mm} \times 200\,\text{mm} \times 66\,\text{mm}$, corresponding to an aspect ratio $\Gamma = L/H = 3$, similar to Zwirner *et al.* (2022) for non-magnetic convection studies. The temperature gradient is imposed between two vertical copper plates with integrated channels through which water is pumped at a preset temperature and flow rate. The sidewalls are made of 30 mm thick PVC. To minimise thermal losses, the entire convection cell is insulated with closed-cell foam. The temperature difference between the copper plates varies in the range $0.54\,\text{K} \leqslant \Delta T \leqslant 12.8\,\text{K}$ corresponding to a Rayleigh number range of $1.48 \times 10^6 \leqslant Ra \leqslant 3.54 \times 10^7$. The convection cell is situated between the pole pieces of a DC electromagnet which generates a nearly homogeneous horizontal magnetic field $\mathbf{B} = B\mathbf{e_y}$ across the volume of the convection cell (less than 5 % deviation). The magnetic field strength is set in the range $29\,\text{mT} \leqslant B \leqslant 173\,\text{mT}$ corresponding to a Chandrasekhar number range of $2.0 \times 10^2 \leqslant Q \leqslant 1.86 \times 10^6$.

Fluid velocities are measured by ultrasonic Doppler velocimetry (UDV) which enables non-invasive velocity measurements in opaque fluids like liquid metals (Takeda 1987; Brito *et al.* 2001; Eckert, Cramer & Gerbeth 2007). The instrument DOP3010 (Signal Processing SA) is equipped with ultrasonic transducers (8 MHz, TR0805SS) and acquires instantaneous velocity profiles along the propagation direction of the ultrasound beam with an acquisition frequency of 1 Hz and a spatial resolution of approximately 1.5 mm in the direction of the ultrasound propagation and approximately 5–8 mm perpendicular to

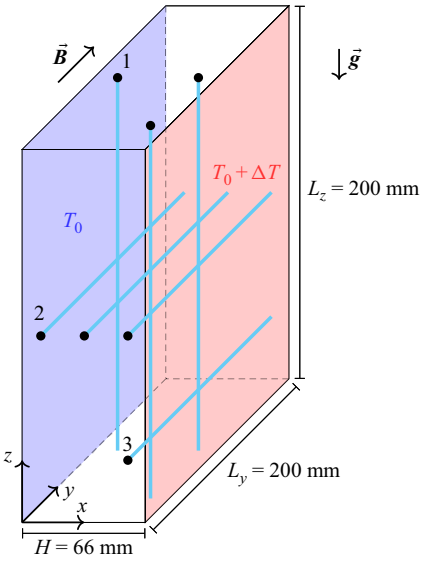

Figure 1. Schematic of the experimental set-up with UDV sensor positions.

the beam. The experimental set-up is instrumented with a total of seven UDV probes, the measuring lines of which are shown as blue lines in figure 1.

Three probes measure the vertical flow velocity u_z and the other four the horizontal velocity u_y parallel to the magnetic field. For both vertical and horizontal directions, sensors are positioned near the hot and cold plates, on the centre plane and in a corner (at $L/5$). All transducers are in direct contact with the liquid metal.

The temperature difference ΔT of the heated and the cooled plates is obtained from two sets of nine thermocouples (type K, calibrated to an accuracy better than 0.05 K), located in each of the copper plates. The convective heat transport is given by the dimensionless Nusselt number, $Nu = \dot{\Phi}/\dot{\Phi}_{cond}$. Here, $\dot{\Phi}_{cond} = \lambda L^2 \Delta T/H$ denotes the conductive heat flux, with λ being the thermal conductivity of the liquid metal, and $\dot{\Phi} = \rho c_p \dot{V}(T_{in} - T_{out})$ is the total heat flux injected at the hot plate and removed from the cold plate, where c_p is the isobaric heat capacity of water. The total heat flux is determined by the flow rate $\dot{V}$ and the temperature change $(T_{in} - T_{out})$ of the circulating water inside the hot (or cold) copper heat exchangers (Schindler *et al.* 2022; Wondrak *et al.* 2023). The water temperatures are measured with high precision PT100 sensors, with a precision better than 0.01 K, and its flow rate with an axial turbine flow sensor (SIKA VTH15) with a measurement uncertainty of 1 %.

The thermal conductivity of copper is approximately 16 times higher than that of GaInSn. In experiments, a higher Nusselt number reduces the effective difference in thermal conductivity between the wall material and the convective flow. This relationship can be assessed using the Biot number (*Bi*) (Özışık 1993; Verzicco 2004), which indicates the ratio of the thermal (conductive) resistance of the copper plate to the thermal transfer resistance of the adjacent fluid and is defined as

$$Bi = Nu \times (\lambda/\lambda_{Cu}) \times (H_{Cu}/H), \tag{2.1}$$

where λ and λ_{Cu} represent the thermal conductivities of the liquid metal and copper, respectively, while H_{Cu} is the thickness of the copper between the water channels and

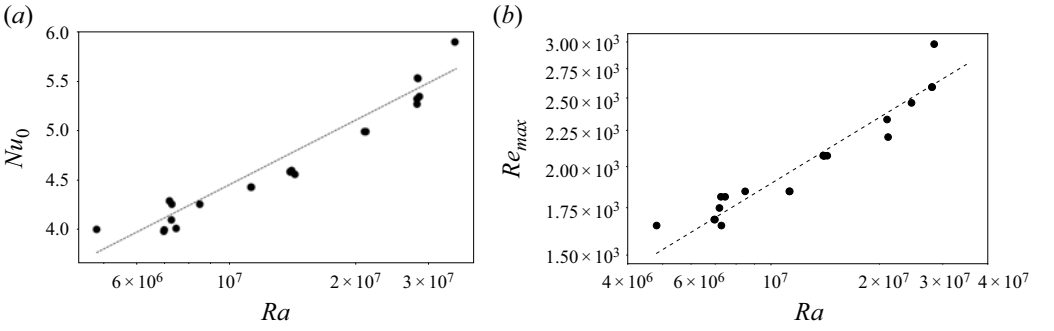

Figure 2. (*a*) Nusselt number Nu_0 against Rayleigh number Ra for $Q=0$. Dashed line fit $f=(0.19\pm0.03)Ra^{0.19\pm0.01}$. (*b*) Vertical Reynolds number Re against Rayleigh number Ra for $Q=0$. Dashed line fit $(12.3\pm0.03)Ra^{0.31\pm0.03}$.

the liquid metal surface. For $Bi<<1$, the boundary conditions can be assumed to be isothermal (Xu, Horn & Aurnou 2022). In our experiments, the Biot number is in the range $0.04\leqslant Bi\leqslant 0.06$, which is sufficiently small to justify the assumption of near-isothermal boundary conditions.

In the following sections, we use dimensionless values, where the plate length L, the free-fall velocity $u_{ff}=\sqrt{\alpha g\Delta T L}$ and the free-fall time $t_{ff}=L/u_{ff}$ are taken as characteristic scales for length, velocity and time, respectively.

3. Results

Systematic investigations are performed in a wide range of the $Ra-Q$ parameter space (see also figure 7). All measurements were conducted in the quasi-steady-state thermal regime, i.e. after changes to the experimental parameters, the acquisition is not started until the temperature gradient between the tempered plates has reached a stationary value.

3.1. *Non-magnetic vertical convection*

Non-magnetic VC has been studied recently by experimental, numerical and analytical approaches (Zwirner *et al.* 2022). We briefly present experimental results obtained with the experimental set-up without a magnetic field ($Q=0$). This configuration serves as a benchmark for our measurement methods as well as a reference for the magnetic cases. The entire Ra range has been investigated for both non-magnetic and magnetic configurations.

Measured Nusselt numbers Nu_0 are shown in figure 2(*a*) and scale approximately as $\propto Ra^{0.19\pm0.01}$. The exponent is slightly lower than the value suggested by Zwirner *et al.* (2022) who showed a slightly steeper scaling. Analytical models predict a scaling around $Ra^{1/4}$ (Shishkina 2016), which is based on an assumption of laminar VC with confined boundary layers. This prediction is in fairly good agreement with our measurements. We note that Ng *et al.* (2015) studied turbulent VC in large aspect ratio cells and observed a scaling closer to $Nu\propto Ra^{0.31}$, which they attribute to enhanced transport in the turbulent regime.

The Reynolds number is calculated on the basis of the averaged maximum velocity from a selected UDV sensor. The noise in the data is taken into account in such a way that 90 % of all measured velocity values are below the determined maximum value. The vertical Reynolds number Re_0 calculated with velocity values measured by sensor 1 is shown in figure 2(*b*). The data scale as $Re_0\propto Ra^{0.31\pm0.03}$ (fit in dashed line in figure 2*b*). The measured exponent is lower than the one proposed by Zwirner *et al.* (2022),

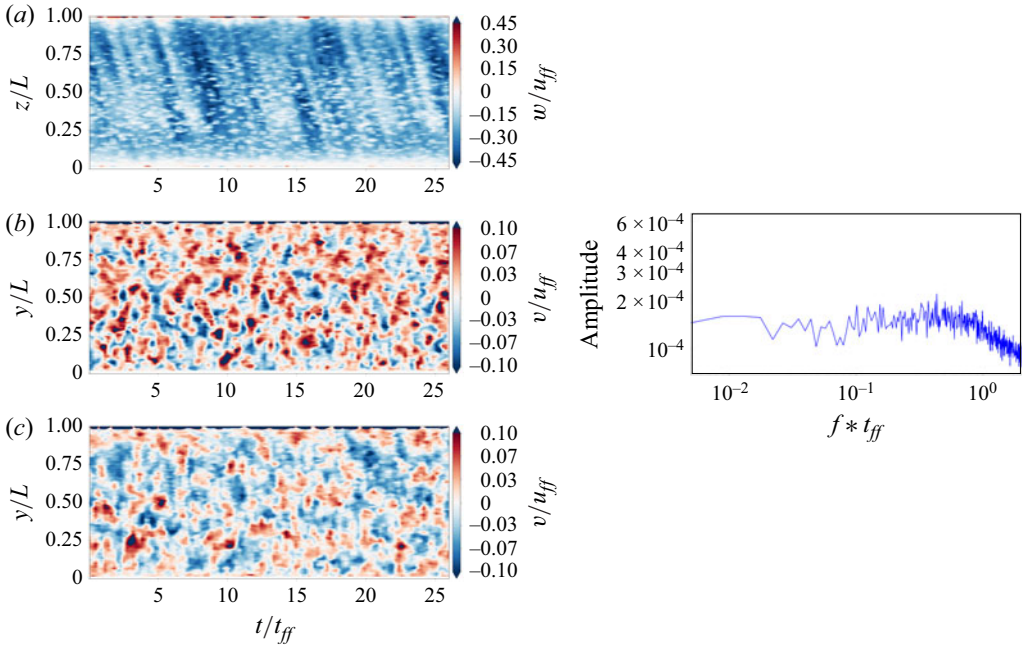

Figure 3. Left: spatio-temporal evolution of the velocity at $Ra = 7 \times 10^6$, $Q = 0$. (*a*) vertical velocity w from sensor 1 (cold plate, centre), (*b*) horizontal velocity v from sensor 2 (cold plate, centre), (*c*) horizontal velocity v from sensor 3 (hot plate, corner). Corresponding measuring lines are shown in figure 1. Velocity follows the direction of the respective y- and z-axes, as drawn in figure 1. Right: depth-averaged velocity spectra of sensor 2. Decay at higher frequency corresponds to the turbulent dissipation.

but consistent with recent analytical work from Ching (2023), who obtained a scaling of $Ra^{1/3}$ for vertical velocities in turbulent VC at large aspect ratio. It should be noted that, while the prediction by Shishkina (2016) assumes laminar convection in a confined geometry, Ching (2023) assumes fully turbulent convection in a large aspect ratio domain. Since our experimental configuration involves a moderate aspect ratio and Reynolds numbers that may not yet correspond to fully developed turbulence, direct comparison with these theoretical scalings must be made with caution. The influence of confinement and the transitional state of the flow may cause deviations from ideal laminar or turbulent scaling predictions.

Flow structures measured by UDV sensors are shown in figure 3 for sensors 1–3, top to bottom. The top panel (vertical component w from sensor 1) shows the vertical downward flow, recorded near the cold plate. This flow presents some non-periodic amplitude variations, with velocities up to approximately 0.45 times the free-fall velocity u_{ff}. Middle and bottom panels show the horizontal velocity along the y component and present small-scale structures in both space, with a length scale of around $0.2L$, and in time, with a life time of around one free-fall time t_{ff}. We interpret these structures as turbulent isotropic small-scale eddies. They show no preferred time scale, as confirmed by the power spectrum of the velocity which is flat until the inertial range (figure 3, right). The clear manifestation of the inertial range also shows very clearly that we have reached the fully developed turbulent regime for our Ra region, which is consistent with previous experimental work for both RBC and VC (Akashi *et al.* 2019; Ren *et al.* 2022; Zwirner *et al.* 2022).

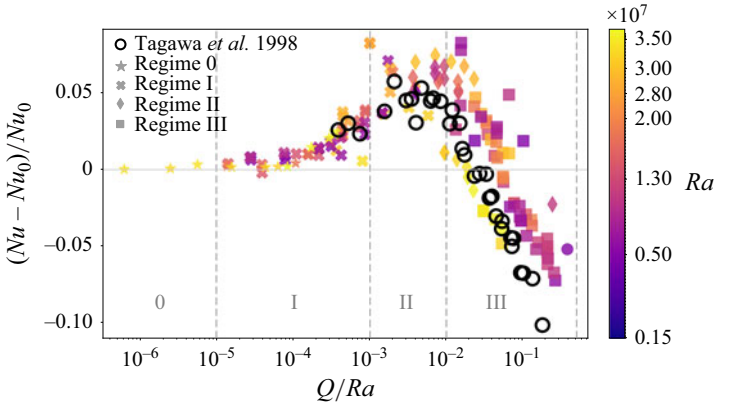

Figure 4. Normalised Nusselt number vs. Q/Ra. The diagram is divided into zones for different flow regimes by dashed lines. The respective flow regimes are determined from the flow measurements (see figure 6) and are presented later in § 3. Data from Tagawa & Ozoe (1998) are reported as open circles.

3.2. *Global transport properties in magneto-convection*

Global heat transfer is a well-studied standard reference parameter to characterise thermal convection in magneto-convection The normalised Nusselt number Nu_B is usually considered, which is defined as $(Nu - Nu_0)/Nu_0$, with Nu_0 as the Nusselt number for the non-magnetic case at the same Ra. In the case of magneto-convection, the characteristic magnitude of the velocity is determined by the balance of buoyancy and electromagnetic forces which can be expressed by the ratio Q/Ra, a parameter equivalent to the magnetic interaction parameter. This normalised Nusselt number is presented as a function of Q/Ra in figure 4. Figure 4 reveals an increase of the convective heat transport in the range $10^{-5} \leqslant Q/Ra \leqslant 10^{-2}$. The value of Nu_B reaches a maximum around $Q/Ra \approx 10^{-2}$ before continuously decreasing with increasing Q/Ra. This behaviour is in general agreement with results reported by previous studies of magneto-convection for both VC (Tagawa & Ozoe 1997, 1998; Authié *et al.* 2003; Burr *et al.* 2003) and RBC (Vogt *et al.* 2021). The experimental data from Tagawa & Ozoe (1998), who studied a cubic cell (64 mm) filled with liquid gallium, for $1.85 \times 10^6 \leqslant Ra \leqslant 4.76 \times 10^6$ and $1.8 \times 10^3 \leqslant Q \leqslant 3.3 \times 10^5$, are included as open circles in figure 4. Comparing our results with previous studies, it becomes obvious that similar effects of a DC magnetic field on heat transport occur for different configurations of thermal convection. An increase of approximately 5 % is observed for VC (this study and Tagawa & Ozoe 1998), whereas a horizontal magnetic field in an RBC geometry shows increases of even up to 25 % (Vogt *et al.* 2021) of the normalised heat transferred compared with their respective non-magnetic value Nu_0.

Figure 5 presents the Ra scaling of both the vertical and horizontal Reynolds numbers defined on the maximum velocities $Re = U_{max} L/\nu$ measured at the sensors 1 and 2, respectively. The Reynolds numbers show a clear Ra dependence, as discussed in previous work (Zwirner *et al.* 2022). In particular, rescaling Re by the predicted dependence for non-magnetic VC $Ra \propto Re^{1/2}$ (Shishkina 2016) collapses the experimental data very well for the entire Ra range, leaving a dependency on Q only, as shown in the insert of figure 5*a*). It seems that the strength of the magnetic field is the relevant parameter. We can only distinguish two different behaviours of Q/Ra: no visible influence of the magnetic field for $Q/Ra < 10^{-5}$ (regime 0), and a monotonic decrease of the Reynolds numbers for $Q/Ra > 10^{-5}$ (regimes I to III), which qualitatively corresponds to the regime separation

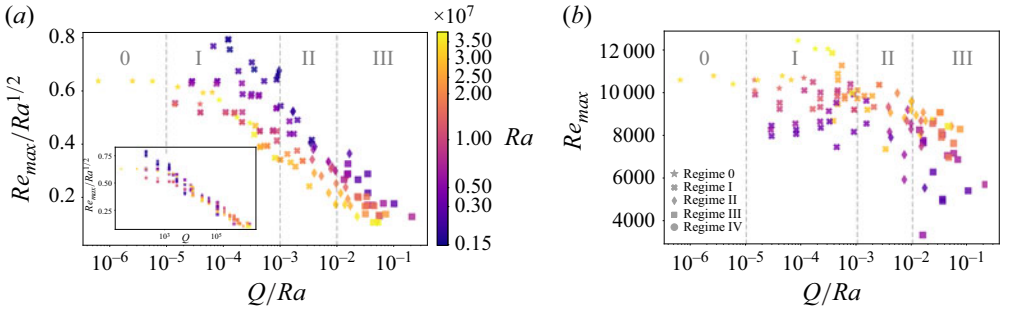

Figure 5. (*a*) Horizontal Reynolds number scaled by $Q/Ra^{1/2}$ for increasing Q/Ra based on maximum velocity measured by sensor 2. Inset shows horizontal Re against Q, where the data collapse, indicating that the magnetic field is the relevant forcing parameter. (*b*) Vertical Reynolds number for increasing Q/Ra based on maximum velocity measured by sensor 1.

observed through heat transfer, although a more precise distinction between regimes I, II and III cannot be made based on horizontal Re data alone.

For the vertical component (figure 5*b*), no clear scaling can be seen from the experimental data. A better collapse of the data is obtained by scaling with $Ra^{1/3}$ (Ching 2023). Interestingly, a change of decreasing slope may be visible around $Q/Ra \approx 10^{-3}$, indicating a potential additional regime separation (between regimes II and III) that is not apparent on the horizontal velocity. In the following section, we focus on the flow structures and suggest a regime classification and discuss how they correspond with the global heat transfer characteristics.

3.3. *Flow structures and regime separation with increasing Q*

In order to get an overall picture of the flow structures and their temporal behaviour, linear velocity profiles were recorded along seven vertical and horizontal measurement lines over a period of 400 free-fall times. In figure 6, we show a selection of spatio-temporal flow patterns composed of a sequence of UDV profiles (vertical axis) measured over time (horizontal axis) for various Chandrasekhar numbers $Q = 1.2 \times 10^4$ (*a–c*), 1.1×10^5 (*e–g*), 1.5×10^6 (*i–k*), at a Rayleigh number of $Ra = 7 \times 10^6$. Velocity and time are non-dimensionalised using the free-fall velocity $u_{ff} = 43.5$ mm/s and the free-fall time $t_{ff} = 4.6$ s. The velocity is set as positive (respectively negative) in the direction along (respectively opposite to) the y–z-axis. We present the velocity fields detected by the sensors 1 (top row), 2 (second row) and 3 (third row). The vertical velocity component measured by sensor 1 reflects the main circulation, which builds up as a coherent roll between the copper plates. A downward flow near the cold plate can be recognised here, the intensity of which is subject to significant fluctuations. The areas of higher velocity can be interpreted as signatures of thermal plumes. These plumes appear to be emitted quite randomly for low Q and then become regularly periodic as Q increases. In the horizontal direction parallel to the magnetic field (sensors 2 and 3), a secondary flow appears, the velocity magnitude of which is significantly lower than the main circulation (approximately 10 % of u_{ff}). Note that the colour scales for the vertical and horizontal components are chosen differently for better visibility. The corresponding sensors on the opposite copper plate (see figure 1) show similar flow patterns of opposing sign for the vertical sensors. This confirms that the problem considered presents a large-scale roll occupying the entire extent of the cell, with similar secondary flows spanning the fluid volume.

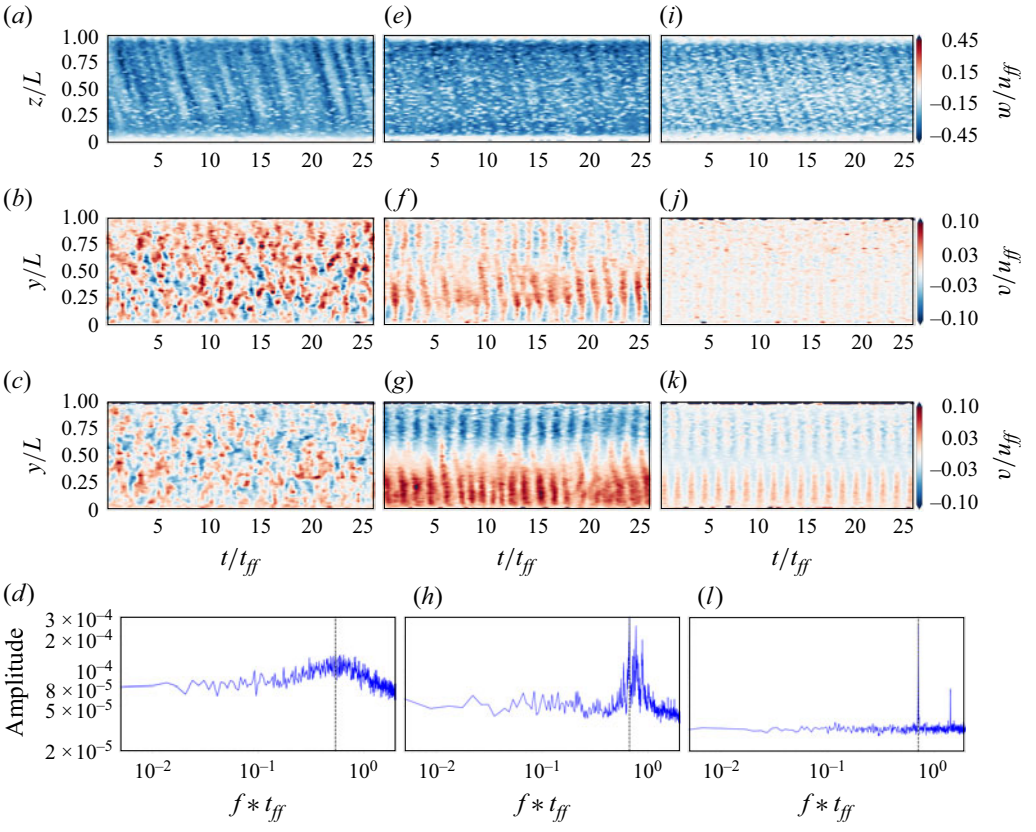

Figure 6. Spatio-temporal evolution of the velocity (UDV) at $Ra = 7 \times 10^6$ for $Q = 1.2 \times 10^4$ (*a–d*), 1.1×10^5 (*e–h*), 1.5×10^6 (*i–l*). Vertical velocities measured by sensor 1, (*a, e, i*), horizontal velocities measured at half-height of the plate by sensor 2 (*b, f, j*) and near the bottom corner by sensor 3 (*c, g, k*). Corresponding measuring lines are shown in figure 1. The direction of the velocity corresponds to the orientation of the respective *y- or z*-axis as drawn in figure 1. Depth-averaged velocity spectra of sensor 2 (*d, h, l*), the dominant frequency $f_0 \times t_{ff} = 0.71$ measured from panel (*l*) is reported for comparison as vertical dashed line across all bottom panels.

At small magnetic fields ($Q \leqslant 10^{-4}$) the secondary flow is composed of small-scale short-lived vortex structures, characteristic of a prevalent isotropic turbulence, which is very similar to the non-magnetic case (figure 3). Significant changes occur for higher Q, in particular the horizontal flow is reorganised into larger coherent structures spanning the entire extent of the convection cell. Both the vertical and horizontal flow patterns are subject to significant oscillations, their regularity becomes clearer with increasing magnetic field strength. Moreover, the horizontal flow profiles recorded at half-height (sensor 2) and in the lower part of the cell near the corner (sensor 3) are remarkably different, which is a clear hint of the existence of a complex three-dimensional flow structure, with a central vortex reconnecting in the corners in a clove pattern, similar to what was proposed by Qin *et al.* (2024).

The bottom row of figure 6 shows corresponding frequency spectra of the horizontal velocity signals (sensor 2), and are a useful tool for differentiating between separate flow regimes. A flat spectrum without any detectable frequency peak is obtained for very small magnetic fields $Q/Ra < 10^{-5}$ (regime 0, not shown here, no visible difference from the

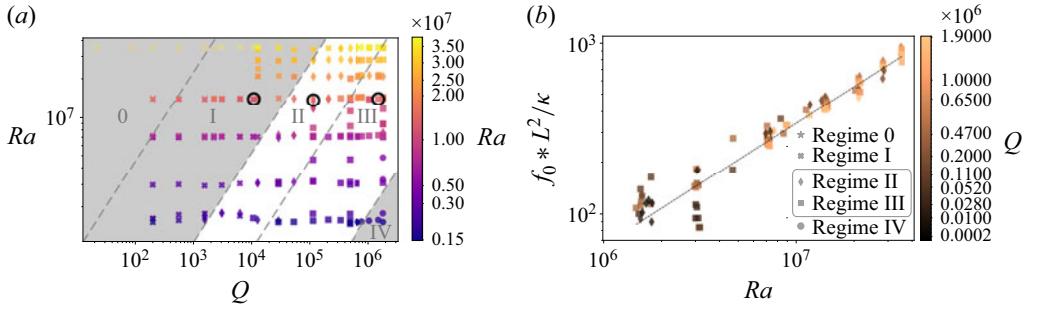

Figure 7. (a) Regime diagram of the measurements performed in the $Ra - Q$ parameter space. Dashed lines $Q \sim Ra^{0.7}$ mark the approximate transition between the flow regimes. Flow structures are characterised by a dominant oscillation in the white areas, and no clear frequency is detected in the grey areas. (*b*) Dominant frequency f_0 normalised by viscous time L^2/κ against Rayleigh number Ra.

non-magnetic field case shown in figure 3, right). This situation does not fundamentally change when a weak magnetic field is applied for $10^{-5} < Q/Ra < 10^{-3}$ (figure 6*d*). However, closer inspection reveals a broad bulge in the power spectra, indicating a preferred time scale. Here, we see the first signs of a loss of isotropy and that is why we refer to this state as regime I. At moderate magnetic field strengths $10^{-3} < Q/Ra < 10^{-2}$ (figure 6*h*), a frequency range of increased energy, from which a several isolated peaks stand out, appears, which we assign to regime II. At high magnetic fields $10^{-3} < Q/Ra < 5 \times 10^{-2}$, regime III, the spectra become sharp and a single well-defined frequency f_0 can be identified (figure 6*l*) (further visible peaks are harmonics of the dominant frequency). The position of f_0 is reported as the dashed line in figures 6(*d*) and 6(*f*), showing that first anisotropy signs seen in earlier regimes are indeed precursors of the main oscillations visible in regime III. The respective results obtained for other UDV sensors are similar. Frequency spectra of temperature sensors show the same behaviour and the same dominant frequencies. For the sake of completeness, it should be mentioned that another regime is observed for $Q/Ra \geq 0.5$, corresponding to a dominant magnetic influence, where no dominant frequency can be detected (regime IV, not shown here).

Figure 7(*a*) provides an overview of the different flow regimes in the $Ra - Q$ parameter space. The measurements shown in figure 6 are highlighted here by a circle. It should be noted that there is no sharp transition between the individual regimes, but the conversions tend to be gradual. The boundary lines between the regimes are estimated by $Q \sim Ra^{0.7}$, represented by dashed lines in figure 7(*a*).

This regime separation corresponds to the qualitative global behaviour changes in the Nusselt and Reynolds numbers, as shown in figures 1(*b*) and 5. In particular, first indications for a heat transfer enhancement become visible for regime I. A significantly steeper growth occurs in regime II, while an optimum of heat transfer is achieved in the transition region between regimes II and III, where also the secondary flow reaches its largest length scale. The Hartmann braking becomes dominant in regime III, leading to a distinct decline both in velocity magnitude and heat transfer. Similar regime separations have been documented based on numerical data by Taghikhani (2014) and Wang & Zhou (2019).

A dominant frequency f_0 can be extracted for regimes II and III (white areas in figure 7*a*). Figure 7(*b*) presents the dominant dimensionless frequencies as a function of Ra. A least-square fit (dashed line) gives the scaling relation $f_0 \times L^2/\kappa \approx 3.7 \times 10^{-4} Ra^{0.71 \pm 0.02}$. No obvious dependence on Q is observed, suggesting that oscillations in the flow patterns are a pure hydrodynamic effect that becomes prominent in the presence

of a horizontal magnetic field. Another interesting point is the observation that the power law in figure 7(*b*) suggests an $Ra^{2/3}$ dependence of the characteristic frequency. In this the case, it would mean that any dependence on the length scale L would be eliminated. We are still cautious about drawing further conclusions at this point, since we are not sure whether this statement is tenable in view of the limited amount of data available at only one aspect ratio and the measurement uncertainty of f_0, especially at small values of Ra and Q. However, this point should be pursued in future work.

4. Summary and conclusions

Experimental investigations of liquid metal VC reveal a distinct influence of a horizontal magnetic field on both the flow structures and the heat transfer. The primary flow consists of a large circulation roll between the two heated or cooled copper plates. This circulation is subject to fluctuations that can probably be associated with the emission of individual plumes. In the thermally dominated regime, measurements of the horizontal velocity component reveal small-scale time-varying structures. With increase of the magnetic field, the secondary flow presents the most noticeable effect, as a coherent secondary flow forms perpendicular to the plane of the main circulation, which completely fills the horizontal dimension of the convection cell. Similar flow patterns were recently proposed from numerical simulations by Qin *et al.* (2024). This could be explained by the fact that a moderate horizontal magnetic field can significantly amplify the intensity of the main circulation through an inverse energy cascade which is known for magneto-hydrodynamic turbulence (e.g. Pothérat & Klein 2017; Sommeria & Moreau 1982), where energy is transferred from small-scale three-dimensional turbulence to coherent quasi-two-dimensional vortex structures whose axes are aligned along the field lines. This strengthening of the primary flow, which continues until a quasi-two-dimensional convection roll has completely spread between the Hartmann layers on the walls perpendicular to the magnetic field direction, also drives the secondary flow in the form of Ekman pumping.

The question arises as to the driving force behind the formation of this coherent secondary flow. It is known that the application of magnetic fields promotes the formation of two-dimensional flow structures, which are characterised by vanishing velocity gradients in the direction of the field lines (Sommeria & Moreau 1982). In this case, a strengthening of the main circulation roll and its full expansion between the Hartmann walls perpendicular to the magnetic field is to be expected. The same mechanism also causes the formation of quasi-two-dimensional convection rolls in a $\Gamma = 5$ RBC box under the influence of a horizontal field (Vogt *et al.* 2021; Yang, Vogt & Eckert 2021). For such quasi-two-dimensional roll structures, which are delimited by two parallel walls, the so-called Ekman pumping, which results from the imbalance between the centrifugal forces and the radial pressure gradient in the boundary layers, becomes relevant. A secondary circulation occurs characterised by a converging flow in the boundary layers driving an inward flow mainly along the axis of the primary circulation roll. Why this Ekman pumping is subject to such strong oscillations here, which can even lead to reversals in flow direction, and why the intensity at the lower edge of the main circulation is larger than in its centre, cannot be fully clarified by these measurements.

However, one striking effect of the magnetic field that was not directly predicted is the occurrence of strong oscillations with a main frequency f_0 both in the primary and secondary flows when the thermal forcing and the electromagnetic forces are of the same magnitude. These oscillations are not detected in the limiting cases of a thermally dominated regime at very low magnetic fields $Q/Ra < 10^{-5}$ and a magnetically dominated regime $Q/Ra \geq 0.5$. In the Q/Ra range between these two limiting cases, the

analysis of frequency spectra of the oscillating flow enables a classification into three regimes: regime I which is characterised by the first minor deviations from isotropy where the energy is continuously distributed around f_0; regime II where thermal and magnetic forces are quite balanced, and the energy is distributed over a discrete number of frequencies around a dominating frequency f_0; regime III where magnetic damping (Hartmann braking) becomes prevalent, and the energy is concentrated in a single peak at f_0. Various phases can be identified in the dependence of the Nusselt number Nu on Q/Ra, which show a certain coincidence with the occurrence of the various flow regimes. The Nusselt numbers reach maximum values in the transition range between the force-balanced regime II to the magnetically dominated regime III, thereafter, the heat transfer is continuously reduced with increasing Q.

The experimental results presented here provide novel insights into the structures and dynamics of liquid metal VC under the influence of a horizontal magnetic field. However, we reach technical limits that do not allow us to completely reconstruct the structures and disclose the detailed mechanism for the striking periodic oscillations, although the same frequencies can also be found in the temperature signals. Therefore, further investigations are planned, which should include numerical simulations in addition to expanding the experimental set-up with additional sensors. Additional measurement techniques which could give insights to three-dimensional flow would also be interesting to add, such as contactless inductive flow tomography Wondrak *et al.* (2023). In particular, special attention will be given to the interaction between the main circulation, the secondary re-circulation and additional local structures such as corner rolls.

Supplementary material. Supplementary material is available at https://doi.org/10.1017/jfm.2025.10386

Acknowledgements. The authors thank and acknowledge Dr V.S. Galindo for his magnetic field simulation which confirmed the homogeneity of the magnetic field in the set-up.

Funding. This work is supported by the Deutsche Forschungsgemeinschaft (DFG) under grants SH 405/16 and the Priority Programme SPP 1881 'Turbulent superstructures' of the DFG under grants VO 2331/3 and VO 2331/4.

Declaration of interests. The authors report no conflict of interest.

Data availability statement. The data that support the findings of this study are available upon reasonable request from the authors.

Author contributions. S. Singh and S. Su performed the experiments and analysed the data. S. Su and T. V. produced the figures. All authors contributed to data interpretation, reaching conclusions and in writing the paper.

References

Ahlers, G., Grossmann, S. & Lohse, D. 2009 Heat transfer and large scale dynamics in turbulent Rayleigh–Bénard convection. *Rev. Mod. Phys.* **81** (2), 503–537.

Akashi, M., Yanagisawa, T., Tasaka, Y., Vogt, T., Murai, Y. & Eckert, S. 2019 Transition from convection rolls to large-scale cellular structures in turbulent Rayleigh–Bénard convection in a liquid metal layer. *Phys. Rev. Fluids* **4** (3), 033501.

Alchaar, S., Vasseur, P. & Bilgen, E. 1995 Natural convection heat transfer in a rectangular enclosure with a transverse magnetic field. *J. Heat Transfer* **117** (3), 668–673.

Authié, G., Tagawa, T. & Moreau, R. 2003 Buoyant flow in long vertical enclosures in the presence of a strong horizontal magnetic field. Part 2. Finite enclosures. *Eur. J. Mech. – B/Fluids* **22** (3), 203–220.

Bader, S.H. & Zhu, X. 2023 Scaling relations in quasi-static magnetoconvection with a strong vertical magnetic field. *J. Fluid Mech.* **976**, A4.

Batchelor, G.K. 1954 Heat transfer by free convection across a closed cavity between vertical boundaries at different temperatures. *Q. Appl. Maths* **12** (3), 209–233.

BODENSCHATZ, E., PESCH, W. & AHLERS, G. 2000 Recent developments in Rayleigh–Bénard convection. *Annu. Rev. Fluid Mech.* **32** (1), 709–778.

BRITO, D., NATAF, H.-C., CARDIN, P., AUBERT, J. & MASSON, J.-P. 2001 Ultrasonic Doppler velocimetry in liquid gallium. *Exp. Fluids* **31** (6), 653–663.

BURR, U., BARLEON, L., JOCHMANN, P. & TSINOBER, A. 2003 Magnetohydrodynamic convection in a vertical slot with horizontal magnetic field. *J. Fluid Mech.* **475**, 21–40.

CHEN, Y.-M. & PEARLSTEIN, A.J. 1989 Stability of free-convection flows of variable-viscosity fluids in vertical and inclined slots. *J. Fluid Mech.* **198**, 513–541.

CHING, E.S.C. 2023 Heat flux and wall shear stress in large-aspect-ratio turbulent vertical convection. *Phys. Rev. Fluids* **8** (2), L022601.

DAVIDSON, P.A. 1995 Magnetic damping of jets and vortices. *J. Fluid Mech.* **299**, 153–186.

DEREBAIL, R. & KOSTER, J.N. 1997 Numerical simulation of natural convection of gallium in a narrow gap. *Intl J. Heat Mass Transfer* **40** (5), 1169–1180.

ECKERT, S., CRAMER, A. & GERBETH, G. 2007 Velocity measurement techniques for liquid metal flows. In *Fluid Mechanics and Its Applications*, vol. 80. Springer.

GARANDET, J.P., ALBOUSSIERE, T. & MOREAU, R. 1992 Buoyancy driven convection in a rectangular enclosure with a transverse magnetic field. *Intl J. Heat Mass Transfer* **35** (4), 741–748.

GROSSMANN, S. & LOHSE, D. 2000 Scaling in thermal convection: a unifying theory. *J. Fluid Mech.* **407**, 27–56.

GROSSMANN, S. & LOHSE, D. 2002 Prandtl and Rayleigh number dependence of the Reynolds number in turbulent thermal convection. *Phys. Rev. E* **66** (1), 016305.

HENRY, D. & BENHADID, H. 2007 Multiple flow transitions in a box heated from the side in low-Prandtl-number fluids. *Phys. Rev. E* **76** (1), 016314.

HENRY, D. & BUFFAT, M. 1998 Two- and three-dimensional numerical simulations of the transition to oscillatory convection in low-Prandtl-number fluids. *J. Fluid Mech.* **374**, 145–171.

KAKARANTZAS, S.C., BENOS, L.T., SARRIS, I.E., KNAEPEN, B., GRECOS, A.P. & VLACHOS, N.S. 2017 MHD liquid metal flow and heat transfer between vertical coaxial cylinders under horizontal magnetic field. *Intl J. Heat Fluid Flow* **65**, 342–351.

MASUDA, T., TAGAWA, T., ALAM, M.M.A. & HAYAMIZU, Y. 2023 Transition of natural convection of liquid metal in an annular enclosure under a magnetic field. *Phys. Fluids* **35** (1), 014112.

MEDELFEF, A., HENRY, D., BOUABDALLAH, A. & KADDECHE, S. 2019 Bifurcations from steady to quasi-periodic flows in a laterally heated cavity filled with low Prandtl number fluids. *J. Fluid Mech.* **861**, 223–252.

NG, C.S., OOI, A., LOHSE, D. & CHUNG, D. 2015 Vertical natural convection: application of the unifying theory of thermal convection. *J. Fluid Mech.* **764**, 0349–0361.

OKADA, K. & OZOE, H. 1992 Experimental heat transfer rates of natural convection of molten gallium suppressed under an external magnetic field in either the X, Y, or Z direction. *J. Heat Transfer* **114** (1), 107–114.

ÖZIŞIK, M.N. 1993 *Heat Conduction*. John Wiley & Sons.

OZOE, H. & OKADA, K. 1989 The effect of the direction of the external magnetic field on the three-dimensional natural convection in a cubical enclosure. *Intl J. Heat Mass Transfer* **32** (10), 1939–1954.

PANDEY, A., SCHEEL, J.D. & SCHUMACHER, J. 2018 Turbulent superstructures in Rayleigh–Bénard convection. *Nat. Commun.* **9** (1), 2118.

PLEVACHUK, Y., SKLYARCHUK, V., ECKERT, S., GERBETH, G. & NOVAKOVIC, R. 2014 Thermophysical properties of the liquid Ga–In–Sn eutectic alloy. *J. Chem. Engng Data* **59** (3), 757–763.

POTHÉRAT, A. & KLEIN, R. 2017 Do magnetic fields enhance turbulence at low magnetic Reynolds number? *Phys. Rev. Fluids* **2** (6), 063702.

QIN, J.-J., ZHANG, C.-N., ZHENG, L.-Y., MA, W.-T., ZHAO, B.-X. & LIU, D. 2024 Comparison of natural convection in liquid gallium under horizontal and vertical magnetic fields. *Intl Commun. Heat Mass* **159**, 108125.

REN, L., TAO, X., ZHANG, L., NI, M.-J., XIA, K.-Q. & XIE, Y.-C. 2022 Flow states and heat transport in liquid metal convection. *J. Fluid Mech.* **951**, R1.

SCHINDLER, F., ECKERT, S., ZÜRNER, T., SCHUMACHER, J. & VOGT, T. 2022 Collapse of coherent large scale flow in strongly turbulent liquid metal convection. *Phys. Rev. Lett.* **128** (16), 164501.

SHISHKINA, O. 2016 Momentum and heat transport scalings in laminar vertical convection. *Phys. Rev. E* **93** (5), 051102(R).

SOMMERIA, J. & MOREAU, R. 1982 Why, how, and when, MHD turbulence becomes two-dimensional. *J. Fluid Mech.* **118**, 507–518.

STEVENS, R.J.A.M., BLASS, A., ZHU, X., VERZICCO, R. & LOHSE, D. 2018 Turbulent thermal superstructures in Rayleigh–Bénard convection. *Phys. Rev. Fluids* **3** (4), 041501(R).

TAGAWA, T. & OZOE, H. 1997 Enhancement of heat transfer rate by application of a static magnetic field during natural convection of liquid metal in a cube. *J. Heat Transfer* **119** (2), 265–271.

TAGAWA, T. & OZOE, H. 1998 Enhanced heat transfer rate measured for natural convection in liquid gallium in a cubical enclosure under a static magnetic field. *J. Heat Transfer* **120** (4), 1027–1032.

TAGHIKHANI, M.A. 2014 Magnetic field effect on natural convection flow with internal heat generation using fast-method. *J. Appl. Fluid Mech.* **8** (2), 189–196.

TAKEDA, Y. 1987 Measurement of velocity profile of mercury flow by ultrasound Doppler shift method. *Nucl. Technol.* **79** (1), 120–124.

TEIMURAZOV, A., SINGH, S., SU, S., ECKERT, S., SHISHKINA, O. & VOGT, T. 2023 Oscillatory large-scale circulation in liquid-metal thermal convection and its structural unit. *J. Fluid Mech.* **977**, A16.

VERZICCO, R. 2004 Effects of nonperfect thermal sources in turbulent thermal convection. *Phys. Fluids* **16** (6), 1965–1979.

VOGT, T., HORN, S., GRANNAN, A.M. & AURNOU, J.M. 2018 Jump rope vortex in liquid metal convection. *Proc. Natl Acad. Sci. USA* **115** (50), 12674–12679.

VOGT, T., YANG, J.C., SCHINDLER, F. & ECKERT, S. 2021 Free-fall velocities and heat transport enhancement in liquid metal magneto-convection. *J. Fluid Mech.* **915**, A68.

WANG, H.Y., ZHANG, X.D., DING, K.K. & WANG, W. 2010 Numerical simulation of nature convection and heat transfer of the liquid LiPb in cubic enclosure with a magnetic field. *Fusion Engng Des.* **85** (7–9), 1215–1219.

WANG, Q., LOHSE, D. & SHISHKINA, O. 2021 Scaling in internally heated convection: a unifying theory. *Geophys. Res. Lett.* **48** (4), e2020GL091198.

WANG, Z.H., MENG, X. & NI, M.J. 2017 Liquid metal buoyancy driven convection heat transfer in a rectangular enclosure in the presence of a transverse magnetic field. *Intl J. Heat Mass Transfer* **113**, 514–523.

WANG, Z.H. & ZHOU, Z.K. 2019 External natural convection heat transfer of liquid metal under the influence of the magnetic field. *Intl J. Heat Mass Transfer* **134**, 175–184.

WONDRAK, T., SIEGER, M., MITRA, R., SCHINDLER, F., STEFANI, F., VOGT, T. & ECKERT, S. 2023 Three-dimensional flow structures in turbulent Rayleigh–Bénard convection at low Prandtl number $Pr = 0.03$. *J. Fluid Mech.* **974**, A48.

XU, Y., HORN, S. & AURNOU, J.M. 2022 Thermoelectric precession in turbulent magnetoconvection. *J. Fluid Mech.* **930**, A8.

YAN, M., CALKINS, M.A., MAFFEI, S., JULIEN, K., TOBIAS, S.M. & MARTI, P. 2019 Heat transfer and flow regimes in quasi-static magnetoconvection with a vertical magnetic field. *J. Fluid Mech.* **877**, 1186–1206.

YANG, J.C., VOGT, T. & ECKERT, S. 2021 Transition from steady to oscillating convection rolls in Rayleigh–Bénard convection under the influence of a horizontal magnetic field. *Phys. Rev. Fluids* **6** (2), 023502.

ZÜRNER, T., VOGT, T., ECKERT, S. & SCHUMACHER, J. 2018 Local lorentz force and ultrasound Doppler velocimetry in a vertical convection liquid metal flow. *Exp. Fluids* **59** (1), 3.

ZWIRNER, L., EMRAN, M., SCHINDLER, F., SINGH, S., ECKERT, S., VOGT, T. & SHISHKINA, O. 2022 Dynamics and length scales in vertical convection of liquid metals. *J. Fluid Mech.* **932**, A9.